Time-Delayed Second Harmonic Generation

J. H. Brownell, X. Lu, and S. R. Hartmann
Physics Department, Columbia University, New York, New York 10027
(Received 19 May 1995)

Second harmonic generation in Cs vapor is produced by the combined action of a polarized laser pulse and a magnetic field. It is delayed from the 10 ps excitation pulse by several hundred ps. The laser is two-photon resonant with the $6S_{1/2}$-$6D_{3/2}$ transition and initially induces a macroscopic quadrupole moment whose radiation pattern has a null in the forward direction. The magnetic field reshapes this pattern to produce second harmonic light, which is simply a free polarization decay signal evolving in a manner akin to the free induction decay following an adiabatic demagnetization.

PACS numbers: 42.65.Ky, 42.50.Md

Second harmonic generation in symmetric media is forbidden in the electric dipole approximation. Even when electric quadrupole and magnetic dipole terms are included, it is prohibited by angular momentum conservation when pumping collinearly [1,2]. Nevertheless, generation of coherent radiation resonant with the sum or difference of the two pumping frequencies has been achieved in several distinct ways: by applying an external electric or magnetic field [3–7]; by pumping collinearly with large enough peak powers to ionize the medium and thereby producing an electric field in the active volume by charge displacement [8–12]; by angling the two pumping beams with respect to each other [7,13]; and by involving high level states that do not have definite parity because of collisions with neighboring atoms [14,15]. In all these experiments, second harmonic generation has appeared simultaneously with the excitation field.

But the second harmonic process does not need to be instantaneous. Previous experiments performed in an atomic vapor involving two-photon resonant and collinear excitation in the presence of a magnetic field displayed an instantaneous character only because the excitation pulses were long compared with internal relaxation times. A linearly polarized two-photon excitation induces a $|\Delta m| \neq 1$ transition, but only a $|\Delta m| = 1$ transition will result in coherent quadrupole radiation. The magnetic field serves to couple the magnetic sublevels. For long pulse irradiation the analysis involves perturbation theory, and the second harmonic generation is seen as a four-wave-mixing process in which two waves are associated with the laser excitation, one with the magnetic field, and one with the second harmonic radiation. In the short pulse limit the magnetic field can be neglected during the passage of the pulse and only when the pulse has terminated does the magnetic field begin to redistribute the magnetic sublevel populations.

This redistribution produces a free polarization decay (FPD), which is the second harmonic signal. It differs from the conventional FPD [16] in that the transition is two-photon excited rather than single and the FPD starts with zero amplitude and then builds up rather that being born full blown. This delayed maximum is rare in free decay, but not unknown. A similar signature in free induction decay (FID) can be produced after adiabatic demagnetization [17]. Several experiments have shown that, in the parametric wave-mixing regime, collinear sum-frequency and difference-frequency generation with a transverse magnetic field is consistent with the "rotation" of the quadrupole moment [4,5]. Yet, a delay between the excitation and the onset of coherent emission has not been reported.

In our experiment, the $6S_{1/2}$ and $6D_{3/2}$ states of cesium were excited into a coherent superposition by the resonant two-photon absorption of a 10 ps, linearly polarized, transform-limited "pump" pulse at 885 nm. The width of the pump pulse was determined by intensity autocorrelation assuming a hyperbolic secant shape. It was close to being transform limited. A magnetic field of a few hundred gauss was applied transverse ($\hat{\mathbf{x}}$) to both the pump polarization ($\hat{\mathbf{z}}$) and propagation ($\hat{\mathbf{y}}$) directions. The pump pulse was obtained from the output of a synchronously pumped dye laser, which was spectrally filtered and amplified. This pulse was split before the sample cell, and one part was directed into an EG&G FND-100 (FND) photodiode that measured the pump pulse energy. A second part was directed onto a 1 GHz bandwidth EG&G C30921E avalanche photodiode (APD 1), to provide a time reference. A third part was imaged, by a 400 nm focal length achromat lens, at the center of either a $L = 1$ cm path length quartz cell or $L = 2.5$ cm 304–type stainless steel cell with sapphire windows, both containing cesium vapor. The cell was situated in an oven and at the center of a pair of 6 cm diameter Helmholtz coils. These coils, driven by a 250 μs period switched L-C circuit, provided an effectively static magnetic field.

Second harmonic (SH) radiation at 442 nm, emerging from the cell along the direction of the pump, was collimated by a 400 nm focal length lens and directed toward either an RCA C31034 photomultiplier tube (PMT), to measure the total emitted energy, or a second APD (APD 2), to measure the temporal intensity profile. To allow detection of both the fundamental and second har-

0031-9007/95/75(20)/3657(4)$06.00

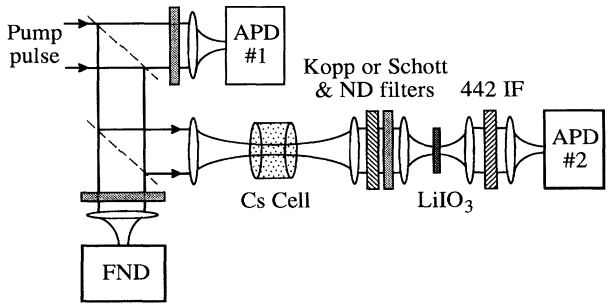

FIG. 1. Schematic detector arrangement. FND and APD 1 monitor pump energy and pump reference temporal profile, respectively. APD 2 include monitors: (1) Cs SH profile with Kopp 4-96 value-pass IF filters; (2) laser pump profile measured at 442 nm by detecting SH from $LiIO_3$ with Schott RG 665 red-pass and 442 IF filters plus ND 1.3 attenuator; and (3) laser pump profile measured at 885 nm with only ND 6.5 attenuator. Each profile measurement includes a trace from APD 1 to fix the temporal displacement of (1), (2), and (3).

monic signals, uncoated lenses and aluminum mirrors were used following the cell. When observing the SH emission from the Cs cell, all radiation except for the SH was blocked from entering the detector by a Kopp 4-96 glass filter and an Andover 100 Å FWHM, 442 nm center bandpass interference filter (442 IF). See Fig. 1.

The SH delay was determined by referring the SH response of APD 2 to the pump pulse response of APD 2. Because the temporal response of the APD detectors was wavelength dependent, a short pulse at 442 nm coincident with the pump was needed as the reference. This short SH pulse was generated in a $LiIO_3$ crystal with the fundamental pump pulse and detected by inserting a Shott RG 665 filter to block the SH from the Cs cell and a ND 1.3 attenuator to protect the $LiIO_3$ crystal. Here again we used the 442 IF filters to block the pump. When all filters were removed and only a ND 6.5 attenuator was inserted, then APD 2 only responded to the pump at 885 nm. As we ran our experiments, the $LiIO_3$ crystal was always in place, located before the APD 2 at the focal plane of a 1:1 magnification, 20 cm focal length telescope.

The outputs of APD 1 and 2 were fed, via cables of unequal length, into a 1 GHz Tek7A29 amplifier mounted in a Tek7104 oscilloscope mainframe. A Tek7B15 time base was triggered externally by the response to the pump pulse of a 35 ps rise time Antel AR-S2 photodiode. A TekDCS01 digitizing camera captured all oscilloscope traces with 20 ps pixel resolution. The APD 1 response was used solely to provide a time reference with which to compare different traces and so eliminate trigger jitter.

The APD 2 responses to the fundamental pump pulse, the SH pulse from the $LiIO_3$ crystal, and the SH from Cs in a 570 field, acquired with different filter-attenuator combinations, are shown in Fig. 2. From this figure, we note that the pump as detected by the 442 nm SH from the $LiIO_3$ is delayed 350 ps from the direct response to the pump at 885 nm and that the actual delay of the SH as produced by the Cs is only half of what we would have measured without making the correction for the response wavelength dependence.

We analyze our data with a model that assumes the following: (1) For the number densities at which we worked [$(5-10)\times10^{14}$ cm^{-3}], the sample is optically thin at the second harmonic wavelength, so radiation reaction could be neglected. (2) Since the pump pulse duration (10 ps) is much shorter than the time taken for SH emission to develop (~300 ps), the initially unpolarized atoms are assumed to be instantaneously excited by the pump pulse into a coherent superposition of the $6S_{1/2}$ and $6D_{3/2}$ states. Immediately after excitation, the amplitudes of the magnetic sublevels coupled by the pump field, which we label α and β for the $6S_{1/2}$ and $6D_{3/2}$ states, respectively, are independent of the sublevel. (3) The range of the magnetic field strength used in our experiments corresponds to transition rates among magnetic sublevels less than 1 GHz. Since the hyperfine splitting of the $6S_{1/2}$ and $6D_{3/2}$ states are 9 and 0.1 GHz, respectively, the hyperfine interaction could be ignored in the $6D_{3/2}$ state evolution but not in the $6S_{1/2}$. (4) The 9 GHz off-resonance magnetic-dipole transitions between the $6S_{1/2}$ hyperfine levels average out and can be neglected. This approximation is valid as long as the Larmor frequency is small compared to 9 GHz, which is not realized from the highest magnetic field strengths used. (5) The nuclear spin contribution to the magnetic sublevel redistribution rate due to the applied magnetic field is to small to consider.

The $\hat{\mathbf{z}}$ polarized SH field amplitude A_F resonant with the $6S_{1/2,F}$-$6D_{3/2}$, $F = 3$ or 4, transition is related to its source by the Maxwell wave equation,

$$\frac{\partial}{\partial y'}A_F(\tau) = 2\pi n(\omega_F/c)^2\hat{\mathbf{z}}\cdot\tilde{\mathbf{Q}}_F(\tau)\cdot\hat{\mathbf{y}} \qquad (1)$$

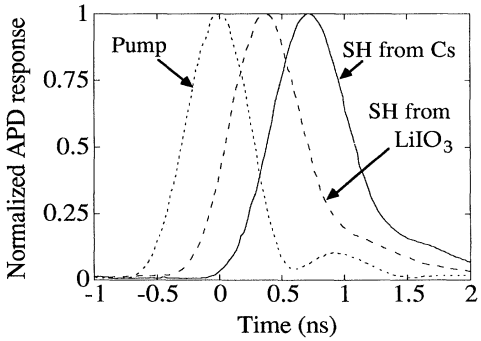

FIG. 2. Temporal profiles (measured by APD 2 detector) of the following: (1) SH from Cs in a 570 G field, (2) laser pump referenced to 442 nm by detecting $LiIO_3$ SH, and (3) laser pump detected at 885 nm. Reference measurements from APD 1 determined temporal displacement of (1), (2), and (3).

in the plane wave, slowly varying envelope approximation with reduced coordinates $\tau = t - y/c$ and $y' = y$, where $\omega_F = \Omega_D - \Omega_{SF}$ (Ω_{S3}, Ω_{S4}, and Ω_D are the $6S_{1/2,F=3}$, $6S_{1/2,F=4}$, and $6D_{3/2}$ level energies) and n is the number density. The moment $\tilde{\mathbf{Q}}_F(\tau)$ is the amplitude associated with the $6S_{1/2,F}$-$6D_{3/2}$ transition of the ensemble average of the quadrupole operator expectation value at time τ. Mixing of the ground and excited state sublevels both contribute to $\hat{\mathbf{z}} \cdot \tilde{\mathbf{Q}}_F(\tau) \cdot \hat{\mathbf{y}}$. From the definitions in [18],

$$\hat{\mathbf{z}} \cdot \tilde{\mathbf{Q}}_F(\tau) \cdot \hat{\mathbf{y}} = i\frac{qd}{32}\sqrt{\frac{9}{2}}|\alpha^*\beta|g_F(\tau),$$

where

$$g_F(\tau) \equiv \left\{\frac{1}{2} + \sum_{m=1}^{F}\cos[\tfrac{1}{4}m\theta(\tau)]\right\}\sin[\tfrac{6}{5}\theta(\tau)] + \left\{\frac{1}{4}\sum_{m=1}^{F} m\sin[\tfrac{1}{4}m\theta(\tau)]\right\}\cos[\tfrac{6}{5}\theta(\tau)],$$

$\theta(\tau) = \mu_B B\tau/\hbar$, B is the magnetic field strength, μ_B is the Bohr magneton, q is the electric charge, and $d = 2.1$ Å^2 is the calculated value of the reduced matrix element E on p. 95 of Ref. [18]. The atomic center-of-mass motion is easily incorporated into the SH field derivation because $\tilde{\mathbf{Q}}_F(\tau)$ is independent of this motion. Under experimental conditions, the $6S_{1/2}$-$6D_{3/2}$ transition is Doppler broadened. Equation (1) correctly describes the field amplitude produced by the subset of atoms with the velocity component $v_y = \hat{\mathbf{y}} \cdot \mathbf{v}$ if the field's frequency includes the Doppler shift. The total field amplitude is the sum over all velocity subsets, which follow a Boltzmann distribution.

Since the apparatus cannot resolve the 9 GHz $6S_{1/2}$ state splitting, the detected SH intensity is averaged over one splitting period. We find

$$I_{\mathrm{SH}}(B,\tau) = \frac{c}{8\pi}\sum_{F=3}^{4}|A_F(\tau)|^2 e^{-(\pi/2)(\tau/T_2^*)^2} = \frac{9\pi}{4096}[nqd(\omega_{\mathrm{DS}}/c)^2]^2 cL^2|\alpha^*\beta|^2 G(B,\tau), \quad (2)$$

where

$$G(B,\tau) = e^{-(\pi/2)(\tau/T_2^*)^2}\sum_{F=3}^{4}|g_F(\tau)|^2,$$

$$(T_2^*)^{-1} = (\omega_{\mathrm{DS}}/c)\sqrt{2kT/\pi M},$$

M is the atom mass, k is the Boltzmann constant, and T is the temperature. Note that the intensity is zero initially, peaks at a later time inversely dependent on B, and is limited by inhomogeneous decay.

Several characteristics of the SH signal were measured to confirm that indeed it was SH generation that was induced by the magnetic field acting on the coherence excited by two-photon absorption. First, the emission died away as the pump was detuned from two-photon resonance. Second, no emission was observed in the backward direction. Third, no emission occurred when either $B = 0$ or the pump polarization was parallel to $\hat{\mathbf{x}}$. Fourth, the SH polarization was linear and along $\hat{\mathbf{z}}$ when the pump's was as well, and elliptical when the pump polarization was circular. Fifth, for low pump pulse energies, the SH energy was proportional to the square of the pump energy and number density.

Energy and temporal profile data were acquired over a range of magnetic field strengths from 0 to 1300 G. Since the pump pulse energy fluctuated, a wide range of pump energy was sampled by simply recording many laser shots for each value of B. Our measurements (not presented here) of the SH energy as a function of the pump pulse energy followed our calculations (within a scale factor) up to a threshold that increased with increasing magnetic field. The temporal profile data were acquired with the steel cell and a pump beam diameter of 1.5 mm.

Typical normalized APD response to the pump pulse (dotted line), the crystal SH (dashed line), and the Cs vapor SH (solid line) are shown in Fig. 2. Though all three are detector bandwidth limited, they are clearly displaced from each other. To verify that the delay was not a subtle artifact of the APD, the temporal profile of the PMT response to the above three signals was also measured. (The PMT rise time was fast enough to resolve a 250 ps time delay.) In this case, the response to the SH generated in the $LiIO_3$ crystal preceded the pump pulse. Nevertheless the SH delay measurements obtained from the PMT's agreed with those obtained from the APD's albeit with reduced accuracy.

For modest pump powers of 5 kW corresponding to 2×10^{11} photons, we obtained the behavior of the SH delay as a function of the applied magnetic field as shown in Fig. 3. The temporal peak of the theoretical SH intensity curve $G(B,\tau)$ (solid line) is plotted vs B using $T_2^* = 0.5$ ns.

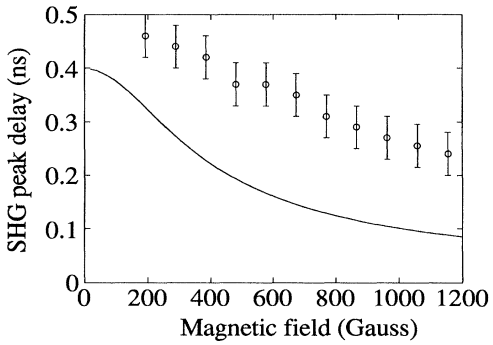

FIG. 3. Delay of second harmonic emission as a function of amplitude of transverse magnetic field. Solid line is calculated from the peak of Eq. (2). Data points were obtained from Cs in the 2.5 cm cell at 200 °C. The 0.05 μJ input to the cell was focused down to a nominal diameter of 1.6 mm.

The two-photon excitation pump pulse that established the coherent superposition between the $6S_{1/2}$ and $6D_{3/2}$ states also resulted in a complete population inversion on the $6D_{3/2}$-$6S_{1/2}$ transition since the $6P_{1/2}$-$6S_{1/2}$ transition is not resonant with the 885 nm radiation of two-photon pump. At the temperatures we worked our Cs sample, although optically thin on the $6D_{3/2}$-$6S_{1/2}$ transition, was optically thick on the $6P_{1/2}$-$6S_{1/2}$ transition. Therefore, subsequent to the two-photon pump pulse the gain on the $6D_{3/2}$-$6P_{1/2}$ transition was much greater than 1 and superfluorescence occurs. This was the subject of a separate study, which will be reported elsewhere. It is relevant to this work since the superfluorescence burst would essentially deplete the $6D_{3/2}$ state population and consequently quench the SH. Fortunately the delay of the superfluorescence burst was considerable, and we could work in the regime where the SH occurred before being appreciably affected by the superfluorescence. The magnetic field dependent threshold energy referred to above is due to the onset of superfluorescence degradation of the $6D_{3/2}$ population before the SH process is complete. Our working below this threshold allowed us to neglect the effect of superfluorescence.

The typical APD response to the SH emission, as shown in Fig. 2, grew from zero (or our background) to peak some 300 ps after the APD response to the SH output from the $LiIO_3$ crystal. As we increased the magnitude of the magnetic field, the delay of the SH decreased. Roughly speaking, the greater the magnetic field the faster the quadrupole moment swings around to fill the null in the radiation pattern set up immediately following the two-photon excitation pulse. In the limit of a weak magnetic field the SH delay is determined by the Doppler broadening. When the magnetic field is less than that producing a delay equal to T_2^* in the absence of Doppler broadening, we expect the delay to become independent of magnetic field. We were not able to make delay measurements in the small magnetic field limit because our signal then became too weak to detect. In other respects the behavior displayed in Fig. 3 agrees with our expectations except for the fact that the measured delays are all too large. The origin of this discrepancy is unknown at this time. We know that superfluorescence is taking place, but we feel that we work in a regime where it is not important.

We note that the decrease in the delay of SH with increasing magnetic field translates into a decrease in any competition that could be associated with the presence of superfluorescence. Since the delay of the superfluorescence burst is inversely proportional to the gain on the superfluorescence transition, it follows that at higher magnetic fields we should be able to observe SH undisturbed by the superfluorescence at higher values of pump energies. This is in accord with the threshold behavior we noted in our measurements of SH energy vs pump energy.

In conclusion, we have observed second harmonic generation delayed from the short excitation pulse. The SH free polarization decay signal grows from zero and peaks at a time inversely related to the applied magnetic field. This behavior is consistent with the slow, magnetically induced evolution of the quadrupole moment in Cs vapor.

We acknowledge stimulating discussion with Professor R. Friedberg, Professor J. T. Manassah, Professor F. Moshary, and Y. Zhang. This work was supported by the Army Research Office and the National Science Foundation, Grant No. PHY-91-22388.

[1] N. Bloembergen and M. D. Levenson, in *High Resolution Laser Sepctroscopy* (Spring-Verlag, Berlin, 1976), p. 315.
[2] T. Hansch and P. Toschek, Z. Phys. **236**, 373 (1970).
[3] H. Uchiki, H. Nakatsuka, and M. Matsuoka, J. Phys. Soc. Jpn. **52**, 3010 (1983).
[4] H. Uchiki, H. Nakatsuka, and M. Matsuoka, Opt. Commun. **30**, 345 (1979).
[5] M. Matsuoka, H. Nakatsuka, H. Uchiki, and M. Mitsunaga, Phys. Rev. Lett. **38**, 894 (1977).
[6] A. Flusberg, T. Mossberg, and S. R. Hartmann, Phys. Rev. Lett. **38**, 59 (1977).
[7] A. Flusberg, T. Mossberg, and S. R. Hartmann, Phys. Rev. Lett. **38**, 694 (1977).
[8] A. J. Poustie and M. H. Dunn, Phys. Rev. A **47**, 1365 (1993).
[9] M.-H. Lu and J.-H. Tsai, J. Phys. B **23**, 921 (1990).
[10] J. Okada, Y. Fukuda, and M. Matsuoka, J. Phys. Soc. Jpn. **50**, 1301 (1981).
[11] D. S. Bethune, Phys. Rev. A **23**, 3139 (1981).
[12] T. Mossberg, A. Flusberg, and S. R. Hartmann, Opt. Commun. **25**, 121 (1978).
[13] D. S. Bethune, R. W. Smith, and Y. R. Shen, Phys. Rev. Lett. **37**, 431 (1976).
[14] S. S. Vianna and C. B. D. Araujo, Phys. Rev. A **44**, 733 (1991).
[15] S. Dinev, J. Phys. B **21**, 1681 (1988).
[16] R. G. Brewer and R. L. Shoemaker, Phys. Rev. A **6**, 2001 (1972).
[17] A. G. Anderson and S. R. Hartmann, Phys. Rev. **128**, 2023 (1962).
[18] E. U. Condon and G. H. Shortley, *The Theory of Atomic Spectra* (Cambridge University Press, Cambridge, 1957).